Ceramics International **22** (1996) 275–280
Published by Elsevier Science Limited and Techna S.r.l.

0272-8842(95)00092-5
0272-8842/96/$15.00

Sintering Studies of Nanophase Ceramic Oxides Using Small Angle Scattering

Andrew J. Allen,[ab] Gabrielle G. Long,[a] Helen M. Kerch,[ac] Susan Krueger,[a] Ganesh Skandan,[d] Horst Hahn[de] & John C. Parker[f]

[a]Materials Science and Engineering Laboratory, National Institute of Standards and Technology, Gaithersburg, Maryland, USA
[b]Department of Materials and Nuclear Engineering, University of Maryland, College Park, Maryland, USA
[c]Office of Basic Energy Sciences, United States Department of Energy, Germantown, Maryland, USA
[d]Department of Mechanics and Materials Science, Rutgers University, Piscataway, New Jersey, USA
[e]Department of Materials Science, Technische Hochschule Darmstadt, Darmstadt, Germany
[f]Nanophase Technologies Corporation, Burr Ridge, Illinois, USA

(Received 7 June 1995; accepted 20 July 1995)

Abstract: The microstructure evolution during sintering of nanophase ceramics has been followed using small-angle neutron and X-ray scattering. These techniques enable material microstructure parameters and surface areas to be measured nondestructively, and have been applied to study the effects of different sintering temperatures, pressures and additives. Depending on the sintered density, the scattering data from nanophase materials exhibit Porod scattering associated with the high surface area, scattering from the nanometer-size grains and pores, and interparticle interference scattering. By using samples of sufficient size and uniformity to permit absolute calibration of the scattering data, it has been possible to develop a fully quantitative microstructure model. Studies of nanophase yttria (powder, prepared by Nanophase Technologies Corporation, Burr Ridge, IL) and zirconia (powder, prepared at Rutgers University, Piscataway, NJ) are discussed, and it is shown how small-angle scattering, in conjunction with density measurements, electron microscopy and X-ray diffraction, provides a unique probe of the statistically representative microstructures present in these novel materials.

1 INTRODUCTION

The potential of nanophase ceramic materials, both as intermediate process–product (offering good formability before final heat treatment), and as final product (offering enhanced mechanical properties for low temperature applications), depends on gaining a better understanding and control of the microstructure evolution during processing. While suitably uniform nanophase powder materials are becoming increasingly available, challenges remain in the fabrication of fully dense product.[1] In particular, as with other ceramic systems, there is a need to better characterize the microstructure evolution as the sintering parameters are varied. The pore and grain size distributions and the grain/pore surface area (related to grain boundary closure) need to be characterized as a function of sintered density under different sintering conditions. The effects of phase transformations, pressure-, vacuum- and air-sintering are all of interest for nanophase ceramic systems.

It is important to obtain quantitative statistical information, which is representative of the overall microstructure, to complement the detailed qualitative information of electron microscopy, which is localized over a few grains. Small-angle scattering is one technique that can give such a nondestructive statistical account of the representative microstructure. However, until recently it has been difficult to obtain absolute calibrations of the scattering data, because of the challenges faced in producing suitably sized uniform samples.[2]

Here, we present small-angle neutron scattering (SANS) data for nanophase yttria (n-Y_2O_3) and nanophase zirconia (n-ZrO_2). We discuss how absolute calibration of SANS reveals it to be dominated by grain–pore interface scattering. By applying a microstructure model in SANS studies, supplemented with ultra-high-resolution small-angle X-ray scattering (USAXS), the microstructure evolution of n-ZrO_2 during sintering has been characterized. We present results for some key microstructure parameters, and review the future potential of such studies.

2 EXPERIMENTAL DISCUSSION

2.1 Nanophase materials

The n-Y_2O_3 studied was prepared using the inert gas phase condensation process.[3] Precursor yttrium metal was evaporated from a tungsten crucible in a low pressure helium atmosphere of 1333 Pa (10 Torr). A rotating cold finger, placed some 200 mm away, collected condensate from the convecting precursor vapors as nanosized metal grains. Once condensation was complete, the helium was removed and pure oxygen gas introduced into the chamber. This resulted in an oxidizing exothermic reaction, converting the yttrium nanoparticles into n-Y_2O_3 powder with a grain size of approximately 6 nm (as confirmed by SANS, X-ray diffraction (XRD) and scanning electron microscopy (SEM)). The n-Y_2O_3 powder was consolidated (at Rutgers) into 0.5–2 mm thick pellets with a consolidation pressure of 500 MPa at room temperature (as-pressed samples) and at 550°C for 3 h (hot-pressed samples). The exact grain sizes and pressed sample densities ($\approx$50% theoretical density (TD)) depended principally on the rate of evaporation from the tungsten crucible and the gas pressures and temperatures. As-pressed (56% TD) samples were sintered in air for 5 h at 600, 900 and 1200°C for this study, giving sintered densities of 71, 85 and nearly 100% TD, respectively.

Fabrication of the n-ZrO_2 was the same as for the n-Y_2O_3, except that ZrO was used in place of yttrium metal. The helium pressure during evaporation was 266 Pa (2 Torr), giving a slow evaporation rate of approximately 8.6 μg s^{-1} (0.5 g min^{-1}). Subsequent consolidation was carried out at a uniaxial pressure of 400 MPa, resulting in 0.5 mm thick pellets of 46% TD. Samples were prepared, sintered in air for 5, 10, 20 and 40 min at 800°C, and sintered *in vacuo* for 2.5, 5, 10, 20 and 40 min at both 800 and 850°C. The effect of a post-sinter anneal, to recover stoichiometry in vacuum-sintered n-ZrO_2, was also determined.

2.2 Microstructural characterization using small-angle scattering

The principles of small-angle scattering are discussed in detail elsewhere.[4] In the present experiments, carried out using the NIST/Exxon/University of Minnesota 30 m SANS instrument at the Cold Neutron Research Facility (CNRF), National Institute of Standards and Technology (NIST), a collimated beam of neutrons, of wavelength 0.55 nm for n-Y_2O_3, 1.0 nm for n-ZrO_2, and $\Delta\lambda/\lambda$ resolution 15%, impinged on a parallel-sided sample, $\approx$0.5 mm thick and 3–8 mm in diameter. A small component of the incident beam was scattered out of the straight-through beam direction by inhomogeneities in the sample microstructure, and the scattered component was registered on the instrument's two-dimensional detector. The scattering data were corrected for empty beam and background counts, calibrated against a scattering standard, and radially summed. By changing the instrument configuration, data were obtained over an overall range of the scattering vector, Q ($Q=(4\pi/\lambda)\sin\theta$, where 2θ is the angle of scatter), of 0.03–1.4 nm^{-1} for n-Y_2O_3. For n-ZrO_2, the Q range was extended by further experiments using the NSF 30m SANS, also at the CNRF, to give a Q range of 0.025–5.0 nm^{-1}.

Figure 1 shows radially summed scattering intensity data as a function of Q for the sintering study of n-Y_2O_3. These data show many of the hallmarks of SANS from nanophase materials revealed in previous SANS studies,[5] in particular the appearance and later disappearance of an interference peak as the sintered density is increased. Coarsening of the grain/pore morphology at high sintering temperatures is also apparent in the shift in the scattering to lower Q values for the sample

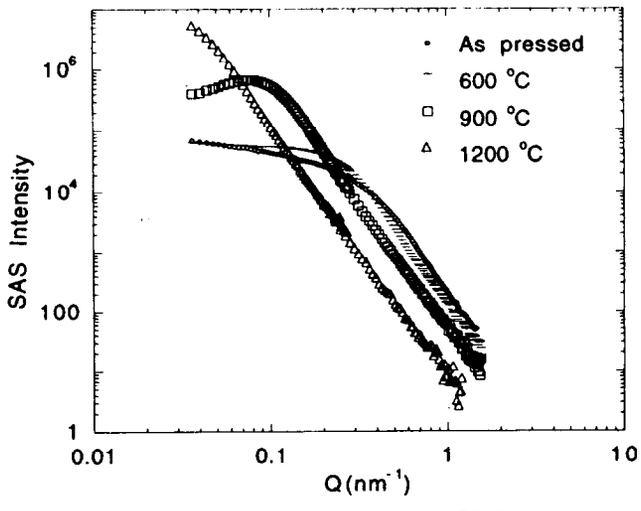

Fig. 1. Typical SANS data for n-Y_2O_3.

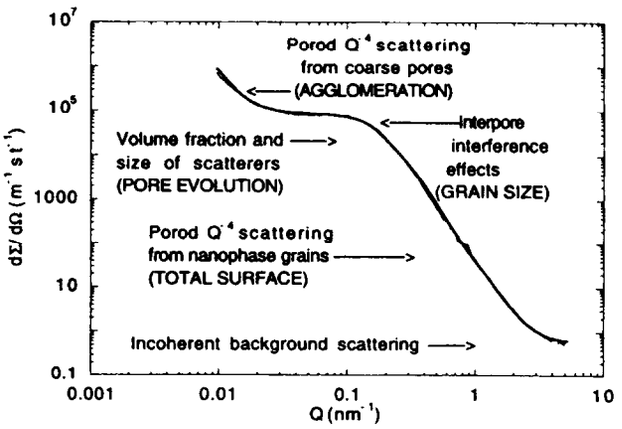

Fig. 2. Absolute calibrated data and fit for n-ZrO_2 sintered *in vacuo* to 91.4% TD.

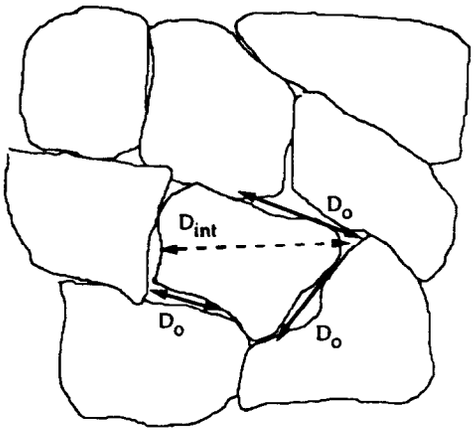

Fig. 3. Microstructure model (numerical averages of D_0 and D_{int} determined).

sintered at 1200°C. Figure 2 shows typical absolute-calibrated scattering cross-section data for n-ZrO_2. The Q range has been extended down to 0.008 nm^{-1} with internormalized USAXS measurements on a specimen, thinned to less than 200 mm. (USAXS measurements were made at the National Synchrotron Light Source on the NIST USAXS instrument[6] using 0.124 nm wavelength X-rays.) Figure 3 indicates how the small-angle scattering is associated with the principal features of the microstructure model, discussed below.

Some basic points can be made before modelling. First, the contribution arising from the pore/grain interface dominates the scattering. Other features, such as a possible low density grain boundary phase, proposed elsewhere,[7] cannot scatter sufficiently strongly to give the SANS observed, while the pore/grain microstructure easily accounts for all of the scattering. Second, the Q^{-4} Porod scattering range at higher Q values in the data can be used to determine the total pore/grain interface surface area, S_v, using Porod's Law[4] ($d\Sigma/d\Omega = 2\pi\Delta\rho^2\ S_v/Q^4$, where $\Delta\rho^2$ is the scattering contrast). This surface can be compared with that deduced from the application of a microstructure model. Third, the characteristics of the SANS data, indicated in Fig. 2, and the changing shape of the data as sintering progresses to higher densities, seem quite general for nanophase materials, regardless of whether a metastable phase transformation is involved during sintering. In the present case, XRD reveals that in n-Y_2O_3, the nanophase grains remain in the metastable monoclinic phase at low temperatures, but above 800°C, where coarsening occurs, this transforms back to the stable cubic phase.[8] In n-ZrO_2, the original powder is mainly in the metastable tetragonal phase, but there is a transformation to the stable monoclinic phase on consolidation.[9] Therefore, there is little or no phase transformation during sintering in n-ZrO_2, even at temperatures at which coarsening occurs. While it is remarkable that the nanophase form of most ceramic materials occurs initially in a metastable phase, this does not seem to have an impact on the microstructure development during sintering. Therefore, the microstructural model that we have developed for the sintering of pure n-ZrO_2 should be applicable, in its essential aspects, to sintering studies in most nanophase ceramic systems.

2.3 Microstructure model for sintering in pure n-ZrO_2

Figure 3 shows the microstructure model developed for the sintering study of n-ZrO_2. The scattering features were assumed to be an approximately log-normal size distribution of mildly oblate pores between the nanophase grains. In the as-pressed material, these pores are polydispersed in size and shape, sufficiently so that no interference scattering is seen. However, as the sintered density is increased and the pores become discrete, interpore interference effects are observed, giving rise to the peak or shoulder seen in the data at intermediate Q values. Eventually, as the porosity is further decreased, the pore population becomes sufficiently dilute for the interference peak to disappear. Existing interference models for SANS either treated a size distribution of interacting spherical scatterers[10] or a monodispersion of spheroids with any pre-set aspect ratio.[11] Our model was developed from the latter, and fits a lognormal size distribution of spheroids[12] for given pre-set aspect ratio, β. The grain size distribution is expected to correlate, at least approximately, with the pore size distribution.

The scattering cross-section for spheroids, of general diameters D_o, D_o, and βD_o, is assumed to follow:

$$d\Sigma/d\Omega = n_{total}P(Q)S(Q) + BGD + P_o \quad (1)$$

where n_{total} is the number of pores per unit sample volume and $P(Q)$ is the scattering form-factor for a single spheroidal pore averaged over all orientations and over the assumed pore lognormal number size distribution. At given Q, the term n_{total} $P(Q)$ is completely characterized by the pre-set spheroidal aspect ratio, the total porosity of the size distribution, ϕ_{pop}, the modal pore diameter, $D_{o\ mode}$, and the median diameter, $D_{o\ med}$, which are fitted directly as parameters in the model. For the n-ZrO_2 sintering studies, best fits were always obtained for mildly oblate aspect ratios, i.e. $\beta = 1/3$ or 1/2. For convenience, fits presented here all have $\beta = 1/3$. From ϕ_{pop}, $D_{o\ mode}$ and $D_{o\ med}$, the population surface area, S_{pop}, and the number-average oblate pore diameter, $D_{o\ avg}$, could be deduced. SEM, XRD and nitrogen desorption studies indicated that $D_{o\ avg}$ gave a rough estimate of the mean grain diameter, D_{grain}. $S(Q)$ contains the interference effects, based on a Percus–Yevick[11] hard-sphere model. Two significant parameters are the local volume (packing) fraction, η, of the interfering pores, and the mean distance between pore centroids, D_{int}. If pores are arranged around grains, D_{int} should also give a measure of D_{grain}. Compared to XRD and SEM results, D_{int} gave a slight overestimate of D_{grain}, but was usually a closer estimate than $D_{o\ avg}$. BGD is the constant incoherent background scattering, and P_o is additional Porod scattering to fit the rise in $d\Sigma/d\Omega$ at small Q. This is attributed to a small number of large pores, associated with a few agglomerated grains.

3 RESULTS AND DISCUSSION OF MODEL

3.1 Model fit results for SAS data

Figure 4 shows data and microstructure model fits for selected samples in the n-ZrO_2 sintering study. While for each sintering condition grain size and density increase moderately with sintering time, the curves shown in Fig. 4 typify the data for each series. Sintering is rapid, and is nearly completed at the earliest sintering times measured (5 min for air-sintering, 2.5 min for the two vacuum-sintered series). For the two vacuum-sintered samples for which USAXS data have been measured at small Q, good fits extend over 3 decades in Q and 7 decades in $d\Sigma/d\Omega$.

For the sintered samples, the rise in the scattering at small Q can be accounted for by a small surface area of order 2.5 m^2 kg^{-1}, or less, associated with a coarse porosity (about 2% of the sample volume) at length-scales well separated from the nanophase scale range of interest, and too large to affect the nanophase microstructure model. For the 'as-pressed' green body, an excellent fit is obtained over much of the range, with any pore-shape β, but the extra scattering at low Q is ignored. Without USAXS data, there is insufficient weight to properly fit this component, which could represent up to 27% of the green body sample volume in coarse pores, not otherwise accounted for.

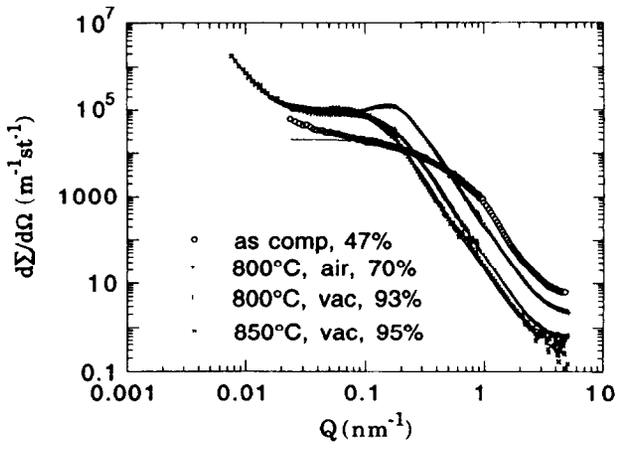

Fig. 4. SANS/USAXS data and fits for selected n-ZrO_2 samples.

In this paper, summary results are presented for the pore/grain size and surface evolution, as a function of the sintered density in n-ZrO_2. Included among the results for isothermal sintering *in vacuo* at 800°C are those for a sample annealed in air, post-sinter, to restore stoichiometry. Such post-sinter annealing was found to have only a negligible effect on the nanophase microstructure.

3.2 Grain size determinations

Figure 5 shows D_{grain}, equated with D_{int} in the microstructure model, as a function of sintered density. For selected samples, mean grain diameters are also shown, based on stereological analysis of SEM images and peak width analysis of XRD scans. These SEM/XRD results are consistently smaller by 10–15% than the corresponding values for D_{int}. However, D_{int} appears to be a better measure of the grain size evolution than the average oblate pore diameter, $D_{o\ avg}$. The latter is typically some 20% more than the SEM/XRD value at low densities, but, as sintering progresses, $D_{o\ avg}$ becomes less than the SEM/XRD grain diameter by as much as 20–25%, at the highest sintered densities of most interest.

It is immediately clear from Fig. 5 that sintering of n-ZrO_2 in air at 800°C has resulted in consider-

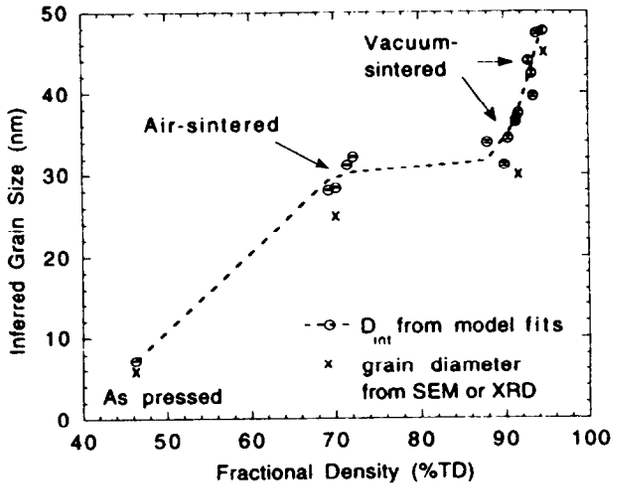

Fig. 5. Grain size vs sintered density for n-ZrO_2.

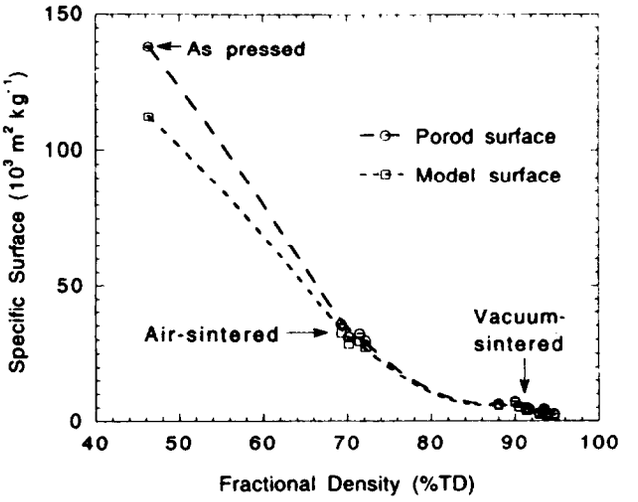

Fig. 6. Specific surface vs sintered density for n-ZrO_2.

able coarsening from 6 to 30 nm, as the density increased from 46% TD to ~70% TD. Vacuum-sintering allows densification to more than 90% TD, with comparable coarsening. Extended vacuum-sintering at 800°C increases the density to 93% TD, with further grain coarsening to 40 nm. At 850°C, extended vacuum-sintering results in slightly higher densities (95% TD), at the expense of grain coarsening to 48 nm. At even higher sintering temperatures, coarsening becomes more marked and the nanophase structure can be lost. Figure 5 suggests that, for the n-ZrO_2 powder used, full density might be achievable with a mean grain size of ~60 nm. Other SANS experiments[13] support this prediction. In fact, recent improvements in the powder fabrication at Rutgers, and the introduction of pressure-sintering, have resulted in near full densities being achieved, with 40 nm grain sizes, in both pure n-ZrO_2 and yttria-stabilized n-ZrO_2, n-YTZP.[14]

3.3 Pore surface evolution

Figure 6 shows the specific pore surface area evolution in n-ZrO_2, as a function of sintered density. The total (Porod) surface area is compared with that deduced from the oblate pore model log-normal number size distributions. As previously discussed, the 'as-pressed' green body contains a substantial volume fraction of coarser pore features, not accounted for by the model. However, in the sintered samples, the model accounts for most of the porosity (where less than 2% of the sample volume is not accounted for), and virtually all of the pore surface area.

Comparison of the grain size (Fig. 5) with the total surface area (Fig. 6) and the size distribution of pores, indicates that the reduction in specific surface area during air-sintering could be almost entirely due to grain boundary losses associated with coarsening. However, in vacuum-sintering, coarsening cannot account for all of the drop in specific surface area. Therefore, if it is assumed that the nanophase pores are predominantly at grain boundaries, in accordance with Fig. 3, some of the grain boundary loss during vacuum-sintering must be due to the closure of grain boundaries between nanophase grains.

4 CONCLUDING DISCUSSION

We have shown how application of a microstructure model to the SANS from nanophase ceramics can be used to quantify their microstructure evolution during sintering. It is only by studies on a wide range of samples that a truly predictive and quantitative picture can emerge. For example, an extended study of isothermal and isochronal sintering is needed to develop and test thermodynamic models for coarsening during the sintering process. To construct a reliable and predictive model for the processing conditions, it is essential to determine microstructure parameters that are statistically representative of the undisturbed microstructures present in each sample. In this paper, we have demonstrated how the use of SANS, with an appropriate microstructure model, can achieve this goal for nanophase ceramics.

ACKNOWLEDGEMENT

This research is partly based upon activities supported by the National Science Foundation under Agreement No. DMR-9122444.

REFERENCES

1. ANDES, R. P., AVERBACK, R. S., BROWN, W. L., BRUS, L. E., GODDARD, W. A., KALDOR, A., LOUIE, S. G., MOSCOVITS, M., PEERCY, P. S., RILEY, S. J., SIEGEL, R. W., SPAEPEN, F. & WANG, Y., *J. Mater. Res.*, **4** (1989) 704.
2. SANDERS, P. G., WEERTMAN, J. R., BARKER, J. G. & SIEGEL, R. W., *Scripta Metall. et Mater.*, **29** (1993) 91.
3. HAHN, H. & AVERBACK, R. S., *J. Appl. Phys.*, **67** (1990) 1113.
4. POROD, G., In *Small-Angle X-ray Scattering*, ed. O. Glatter and O. Kratky. Academic Press, London, 1982, Chap. 2.
5. EPPERSON, J. E., SIEGEL, R. W., WHITE, J. W., EASTMAN, J. A., LIAO, Y. X. & NARAYANASAMY, A., *Mat. Res. Soc. Symp. Proc.*, **166** (1990) 87.
6. LONG, G. G., JEMIAN, P. R., WEERTMAN, J. R., BLACK, D. R., BURDETTE, H. E. & SPAL, R. D., *J. Appl. Cryst.*, **23** (1991) 30.
7. ZHU, X., BIRRINGER, R., HERR, U. & GLEITER, H., *Phys. Rev. B*, **35** (1987) 9085.
8. SKANDAN, G., FOSTER, C. M., FRASE, H., ALI, M. N., PARKER, J. C. & HAHN, H., *Nanostr. Mater.*, **1** (1992) 313.
9. SKANDAN, G., HAHN, H., RODDY, M. & CANNON, W. R., *J. Am. Ceram. Soc.*, **77** (1994) 1706.
10. PEDERSEN, J. S., *Phys. Rev. B*, **47** (1993) 657.
11. GRIFFITH, W. L., TRIOLO, R. & COMPERE, A. L., *Phys. Rev. A*, **35** (1987) 2200.
12. JOHNSON, N. L. & KOTZ, S., *Continuous Univariate Distributions—I.* Houghton-Mifflin, Boston, 1970, Chap. 14.
13. ALLEN, A. J., KRUEGER, S., SKANDAN, G., LONG, G. G., HAHN, H., KERCH, H. M., PARKER, J. C. & ALI, M. N., *J. Am. Ceram. Soc.* (in press).
14. ALLEN, A. J., KRUEGER, S., KERCH, H. M., HAHN, H. & SKANDAN, G., *Nanostr. Mater.*, **7** (1996) 113–26.